Self-assembly of oxidation-responsive polyethylene glycol-paclitaxel prodrug for cancer chemotherapy

Chengyuan Dong, Quan Zhou, Jiajia Xiang, Fusheng Liu, Zhuxian Zhou, Youqing Shen

PII: S0168-3659(20)30128-0

DOI: https://doi.org/10.1016/j.jconrel.2020.02.038

Reference: COREL 10191

To appear in: *Journal of Controlled Release*

Received date: 17 December 2019

Revised date: 19 February 2020

Accepted date: 24 February 2020

Please cite this article as: C. Dong, Q. Zhou, J. Xiang, et al., Self-assembly of oxidation-responsive polyethylene glycol-paclitaxel prodrug for cancer chemotherapy, *Journal of Controlled Release* (2020), https://doi.org/10.1016/j.jconrel.2020.02.038

Self-Assembly of Oxidation-Responsive Polyethylene Glycol-Paclitaxel Prodrug for Cancer Chemotherapy

Chengyuan Dong[1ǂ], Quan Zhou[2ǂ], Jiajia Xiang[2]*, Fusheng Liu[1]*, Zhuxian Zhou[2]*, and Youqing Shen[2]

1. Brain Tumor Research Center, Beijing Neurosurgical Institute, Capital Medical University; Department of Neurosurgery, Beijing Tiantan Hospital Affiliated to Capital Medical University; Beijing Laboratory of Biomedical Materials, Beijing 100070, P. R. China

2. Center for Bionanoengineering and Key Laboratory of Biomass Chemical Engineering of Ministry of Education, College of Chemical and Biological Engineering, Zhejiang University, Hangzhou, China 310007

*Corresponding author's E-mail address: xiang_jj@zju.edu.cn or liufushengs@hotmail.com, or zhouzx@zju.edu.cn

ǂ Equal contributors

Abstract:

Amphiphilic drug conjugates can self-assemble into nanovehicles for cancer drug delivery, but the key is to design stable yet intracellular labile drug linkers for drug retention during blood circulation but fast intracellular drug release. The conjugation of paclitaxel (PTX) is generally via the ester of its 2'-hydroxyl group, but the ester is either too stable to release PTX in the cytosol or so labile that hydrolyzes during circulation. Herein, we report a *p*-(boronic ester)benzyl-based tumor-specifically cleavable linker for preparing PTX-conjugate with polyethylene glycol (PEG, Mw = 5000 Da) (PEG-B-PTX). The amphiphilic PEG-B-PTX self-assembled into micelle with an average size of ~50 nm and a PTX loading content of 13.3 wt%. The PEG-B-PTX micelles were very stable at the normal physiological environment and thus circulated long in the blood compartment, but fast dissociated and released PTX in response to the elevated reactive-oxygen species (ROS) level in tumors. The

conjugate micelles showed significantly improved antitumor efficiency *in vitro* and *in vivo* against human glioma and breast cancer cells, and reduced toxicity compared to the clinically used Taxol. Thus, the PTX-conjugate micelles were characteristic of well-characterized chemical structure and nanostructure, precise and reproducible drug loading efficiency (i.e., 100%) and fixed loading content, high PTX loading content due to PTX itself as part of the carrier, no burst drug release, and easy and reproducible fabrication of the micelles, which are all essential for clinical translation.

Keywords: ROS-responsive linker, polymer-drug conjugate, paclitaxel prodrug, self-assembly prodrug, prodrug micelles.

1. Introduction

Paclitaxel (PTX) is a potent antineoplastic agent for the treatment of various cancers, including breast, lung, and ovarian carcinoma [1, 2]. However, its low water solubility, significant systemic toxicity, and acquired drug resistance are its drawbacks in clinical applications. Various PTX nanoformulations have been developed to address these challenges [3-7]. For instance, Abraxane—albumin-bound PTX nanoparticles—shows better pharmacokinetics and enhanced antitumor activity compared to Taxol and was approved by the FDA for the treatment of metastatic breast cancer in 2005 [8]. Another formulation, Genexol-PM, which is PTX loaded in polyethylene glycol-block-polylactide (PEG-PLA) block copolymer micelles, has been marketed in Asia and is in phase III clinical trial in the USA for the treatment of metastatic breast cancer [9, 10]. Nevertheless, current clinically used PTX nanoformulations generally have drawbacks of poor *in vivo* stability, premature release, and only achieve minor improvements in efficacy [11, 12]. Therefore, great efforts have been devoted to designing novel PTX delivery systems responsive to the biological stimuli to control the drug retention/release for improved efficacy and reduced side effects [13-18]; for instance, PTX was conjugated to polymers via labile linkers in response to the tumor microenvironment stimuli such as such as pH [7, 19, 20], reactive oxygen species (ROS) [21-23], glutathione (GSH) [4, 24, 25], and enzymes [26]. Several PTX prodrug formulations now have progressed to clinical

trials [3].

We demonstrated that a hydrophobic drug conjugated with a short water-soluble polymer or peptide chain made the drug amphiphilic and thus self-assembled into nanovehicles for delivery of the drug and even codelivery of other drugs [14, 16, 27]. This amphiphilic prodrug approach shows many advantages, including well-characterized chemical structures, precise and reproducible drug loading efficiency (i.e. 100%), fixed and high drug loading contents due to the drugs themselves as part of the carriers, and easy and reproducible fabrication of the nanovehicles. Very importantly, these nanovehicles are free of burst release problem generally found in physically drug-loaded micelles [27]. Such characters are favorable for clinical translation compared to complicated polymer counterparts [14, 16, 27-29]. Therefore, we proposed that making PTX amphiphilic with short polyethylene glycol (sPEG) would self-assemble into such micelles with the aforementioned characters ready for clinical translation. The conjugation site for PTX is generally via its ester of 2'-OH [30]. In our preliminary work, we prepared sPEG-PTX prodrugs via the 2'-OH esters of different carboxylic acids. The prodrugs using the aliphatic acid esters, e.g., succinyl ester, as the linker could form well-defined micelles, but they had a very short blood circulation times due to the fast hydrolysis of these esters, while the prodrugs using the esters of aromatic acids were too stable to hydrolyze even in the presence of esterase. Therefore, a stable but intracellular labile ester of PTX is the key for the PTX prodrug forming stable and long-circulating nanovehicles to maximize therapeutic efficacy and to minimize side effects.

Herein, we report a PEG-B-PTX prodrug with a benzylboronic ester-based ROS-responsive cleavable linker between PEG and PTX **(Scheme 1)**. Very interestingly, the *p*-(boronic ester)benzyl succinyl ester of PTX was very stable, and the PEG-B-PTX was hardly hydrolyzable in normal physiological conditions. On the other hand, benzylboronic ester is known oxidizable by the elevated levels of ROS in tumor and tumor cells [31, 32] to trigger an elimination reaction [33-35]. Thus, the amphiphilic PEG-B-PTX could self-assemble into stable micelles with a size of about 50 nm and circulated long in blood. Once accumulated in tumor, the high

concentration of ROS oxidized the *p*-(boronic ester)benzyl group and induced the subsequent 1,4-elimination reaction, resulting in self-cleavage of the linker to release PTX and quinone as a by-product. The released quinone could deplete intracellular GSH, synergistically killing cancer cells [36, 37]. Compared with commercial Taxol and non-responsive control prodrug, PEG-B-PTX exhibited prolonged circulation time, improved *in vivo* antitumor efficacy, and low side effects on mouse tumor xenograft model. With the aforementioned characters, this conjugate has high potentials for clinical translation.

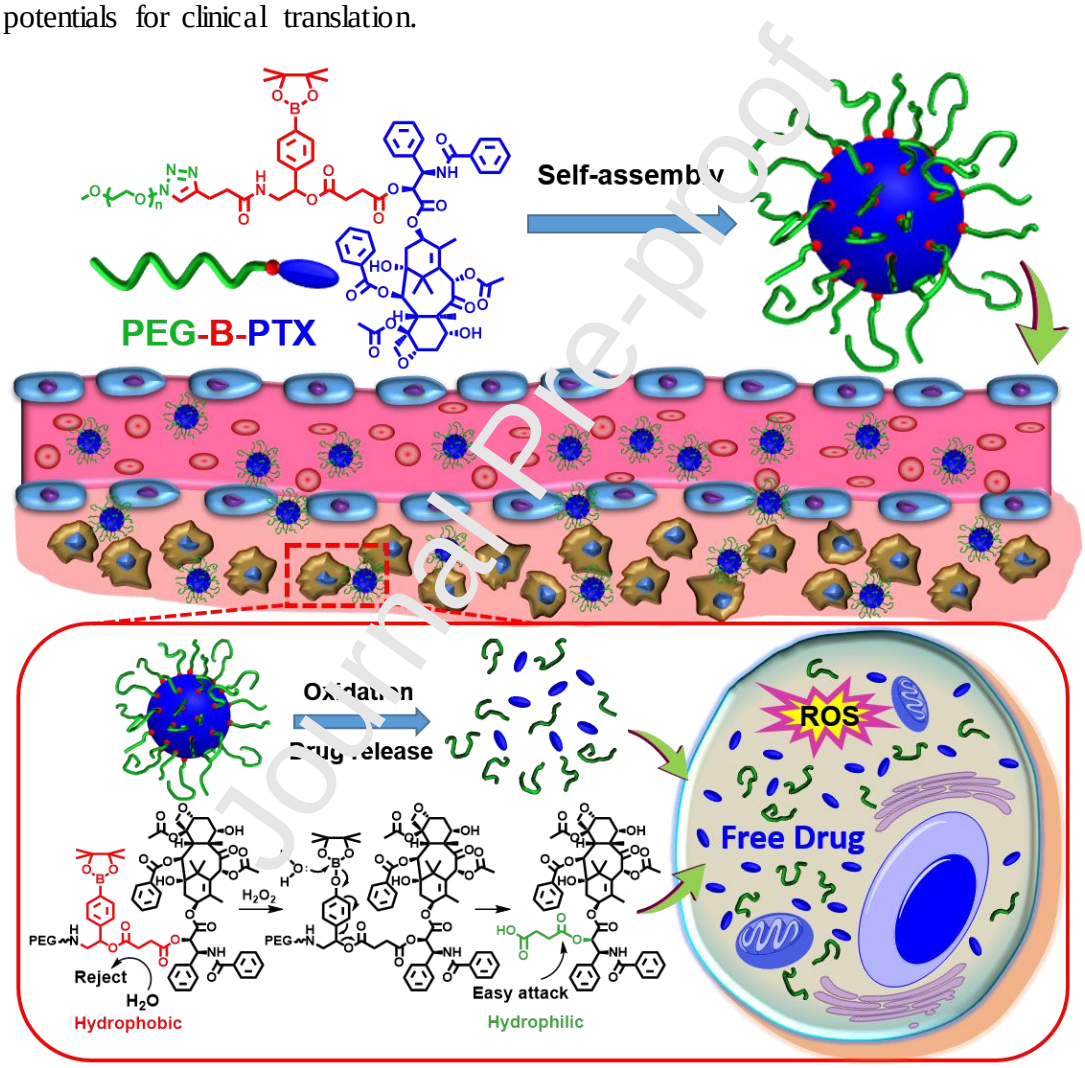

Scheme 1. The chemical structure of the PTX prodrug, PEG-B-PTX, and it's self-assembly into prodrug micelles for the tumor ROS-triggered drug release.

2. Materials and methods

2.1. Materials

2-Amino-4'-bromoacetophenone hydrochloride, di-*tert* butyl dicarbonate, sodium borohydride ($NaBH_4$), bis(pinacolato)diboron, potassium acetate (KOAc), 1'1-bis(diphenylphosphino) ferrocene palladium(II) chloride ($Pd(dppf)Cl_2$·DCM), succinic anhydride, trifluoroacetic acid (TFA), 4-pentynoic acid (PA), N-hydroxysuccinimide (NHS), N,N-dicyclohexylcarbodiimide (DCC), 4-(dimethylamino)pyridine (DMAP), CuBr, and N,N,N,N,-pentamethyldiethylenetriamine (PMDETA) were purchased from Energy Chemical (Shanghai). Paclitaxel (PTX) was purchased from Huilin Bio-tech Co., Ltd. (Xi'an, China). Methoxypoly(ethylene glycol) with a molecular weight of ~5,000 ($mPEG_{5K}$-OH) was purchased from Sigma-Aldrich (Shanghai, China). All other organic solvents were purchased from Sinopharm Chemical Reagent Co. Ltd. (Shanghai, China). Dichloromethane (CH_2Cl_2), tetrahydrofuran (THF), N, N-dimethylformamide (DMF), dioxane, and triethylamine (TEA) were dried over calcium hydride (CaH_2) and distilled before use.

Fetal bovine serum (FBS), trypsin, and RPMI 1640 medium were purchased from GIBCO. 3-(4,5-Dimethylthiazol-2-yl)-2,5-diphenyltetrazolium bromide (MTT) and ROS assay kit (2′,7′-dichlorofluorescein diacetate, DCFH-DA) were purchased from Beyotime Institute of Biotechnology (Shanghai, China). U251 cells were purchased from the Cell Bank of Peking Union Medical College (Beijing, China). Cells were cultured in DMEM (Invitrogen, Carlsbad, CA, USA) with 10 % fetal bovine serum (FBS) 2 mM L-glutamine, 100 U/mL penicillin and 100 μg/mL streptomycin at 37°C in an environment of 5% CO_2. Human breast cancer cell line MCF-7 cells were purchased from American Type Culture Collection (Manassas, USA). Cells were incubated in RPMI-1640 medium containing 10% heat-inactivated FBS and 1% penicillin/streptomycin solution in a humidified atmosphere of 5% CO_2 at 37 ºC. Female BALB/c mice (6-8 weeks) were purchased from the Animal Center of Zhejiang University and maintained under standard conditions. Animal experiments were approved by the Animal Care and Use Committee of Zhejiang University and were carried out in accordance with the institutional guidelines.

2.2. Synthesis of PEG-B-PTX (Scheme 2)

2.2.1 Synthesis of compound 2

Compound 1 (5 g, 23.3 mmol) and di-*tert*-butyl dicarbonate (5.6 g, 25.7 mmol) were dissolved in 100 mL THF at 0 ºC followed by the addition of Et_3N (7.5 mL, 54.1 mmol) in 50 mL THF with a dropping funnel. After the addition was completed, the reaction mixture was heated to 40ºC and stirred for another 2 h. After removing the salts by filtration, the solvent was evaporated, and another 150 mL ethyl acetate was added to dissolve the residues. The organic solution was washed with saturated NH_4Cl aqueous solution, $NaHCO_3$ aqueous solution, and brine, and then dried over anhydrous Na_2SO_4. After removing the solvent, the residues were further purified by flash chromatography affording compound **2** as a white solid (11.5 g, yield: 90%). ^{1}H NMR (400 MHz, $CDCl_3$) δ 7.81 (d, *J* = 8.5 Hz, 2H), 7.63 (d, *J* = 8.5 Hz, 2H), 5.50 (s, 1H), 4.61 (d, *J* = 4.4 Hz, 2H), 1.47 (s, 9H).

Similarly, compound 8 was obtained as a white solid (yield: 73.4%).^{1}H NMR (400 MHz, $CDCl_3$) δ 8.00 – 7.88 (m, 2H), 7.65 – 7.56 (m, 1H), 7.48 (dd, *J* = 10.6, 4.7 Hz, 2H), 5.56 (s, 1H), 4.66 (d, *J* = 4.4 Hz, 2H), 1.47 (s, 9H).

2.2.2 Synthesis of compound 3

To a solution of compound 2 (11.5 g, 36.6 mmol) in methanol, $NaBH_4$ (7.0 g, 185 mmol) was added portion-wise over 10 minutes with vigorous stirring in an ice-salt bath. The mixture was stirred until the TLC monitoring indicated that the reaction of compound 2 was complete. The reaction was next quenched with water addition. Methanol was removed by evaporation, and the aqueous solution was extracted with ethyl acetate (50 mL × 3). The combined organic phase was washed with brine, dried over anhydrous Na_2SO_4, and filtered. After concentration, the crude product was recrystallized in hexane to give compound 3 as a white crystal (10.7 g, yield: 92%). ^{1}H NMR (400 MHz, $CDCl_3$) δ 7.54 – 7.40 (m, 2H), 7.24 (d, *J* = 8.4 Hz, 2H), 4.93 (s, 1H), 4.79 (dd, *J* = 7.2, 2.5 Hz, 1H), 3.51 – 3.34 (m, 1H), 3.31 – 3.09 (m, 1H), 1.44 (s, 9H).

Compound 9 was similarly obtained as a white crystal (yield: 89.2%). ^{1}H NMR (400 MHz, $CDCl_3$) δ 7.41 – 7.26 (m, 5H), 4.96 (s, 1H), 4.88 – 4.74 (m, 1H), 3.46 (s,

1H), 3.32 – 3.15 (m, 1H), 1.44 (s, 9H).

2.2.3 Synthesis of compound 4

Compound 3 (7.6 g, 24.0 mmol), bis(pinacolato)diboron (21.4 g, 84.3 mmol), Pd(dppf)Cl_2·DCM (1.6 g 2.19 mmol), and potassium acetate (12.4 g, 126 mmol) were dissolved in 100 mL 1,4-dioxane under an argon atmosphere. The reaction was heated to 90 ºC and stirred for 12 h. After cooling to room temperature, the undissolved potassium acetate was removed by filtration. After removal of 1,4-dioxane under reduced pressure, the reaction mixture was diluted with EtOAc (150 mL) and washed several times with 1 N HCl and brine. The organic phase was dried over Na_2SO_4, filtered, and the solvent was removed by evaporation. The crude product was purified with flash chromatography to give compound 4 as a white solid (6.5 g, 74.7%). ^{1}H NMR (400 MHz, $CDCl_3$) δ 7.80 (d, *J* = 8.0 Hz, 2H), 7.37 (d, *J* = 7.9 Hz, 2H), 4.96 – 4.77 (m, 2H), 3.49 (s, 1H), 3.30 – 3.07 (m, 2H), 1.44 (s, 9H), 1.34 (s, 12H).

2.2.4 Synthesis of compound 6

4-Pentynoic acid (5.00 g, 51.0 mmol), NHS (6.40 g, 55.6 mmol), and DMAP (1.24 g, 10.1 mmol) were dissolved in 100 mL CH_2Cl_2 at 0 °C followed by the addition of DCC (12.6 g, 61.2 mmol) in 50 mL CH_2Cl_2. The reaction mixture was then warmed to room temperature and stirred for another 2 h. After filtration, the solution was washed with 1 N HCl, saturated $NaHCO_3$ aqueous solution, and brine. The organic phase was dried over anhydrous Na_2SO_4, filtered, and concentrated. The crude product was recrystallized in ethyl acetate/hexane to give PA-NHS as a white crystal with a yield of 76.4%.

Compound 4 (0.50 g, 1.38 mmol) was dissolved in a mixture of CH_2Cl_2/TFA (6 mL, 2:1) and stirred for 6 h at room temperature. Once TLC monitoring indicated complete deprotection, the solvent was removed and additional dry CH_2Cl_2 was added with 1 mL Et_3N. A solution of 5 mL CH_2Cl_2 containing NHS-activated 4-pentynoic acid (PA-NHS, 0.26 g, 1.33 mmol) was added dropwise. After stirring at room temperature for 1 h, the mixture was diluted with 50 mL CH_2Cl_2 and washed successively with 1 N HCl, saturated $NaHCO_3$ aqueous solution, and brine. The separated organic phase was dried over Na_2SO4, filtered, and concentrated. The

resulting residue was further purified by flash chromatograph to give compound 6 as a white solid (0.33 g, yield: 72.2%). ^{1}H NMR (400 MHz, $CDCl_3$) δ 7.79 (d, *J* = 8.0 Hz, 2H), 7.36 (d, *J* = 7.9 Hz, 2H), 6.14 (s, 1H), 4.85 (dd, *J* = 7.6, 3.3 Hz, 1H), 3.71 (ddd, *J* = 14.1, 6.8, 3.4 Hz, 1H), 3.31 (ddd, *J* = 13.8, 7.6, 5.0 Hz, 1H), 2.72 (s, 1H), 2.56 – 2.46 (m, 2H), 2.38 (t, *J* = 7.1 Hz, 2H), 1.99 (t, *J* = 2.6 Hz, 1H), 1.33 (s, 12H). ^{13}C NMR (101 MHz, $CDCl_3$) δ 172.41 (s), 144.73 (s), 135.03 (s), 125.16 (s), 83.88 (s), 82.81 (s), 73.51 (s), 69.53 (s), 47.38 (s), 35.17 (s), 24.87 (s), 14.86 (s).

Compound 11 was similarly obtained as a white solid (yield: 68.0%). ^{1}H NMR (400 MHz, $CDCl_3$) δ 7.42 – 7.28 (m, 5H), 6.76 (s, 1H), 5.82 (s, 1H), 4.83 (s, 1H), 3.62 – 3.28 (m, 4H), 1.40 (d, *J* = 14.3 Hz, 9H). ^{13}C NMR (101 MHz, $CDCl_3$) δ 172.34 (s), 141.63 (s), 128.57 (s), 127.93 (s), 125.86 (s), 82.84 (s), 73.47 (s), 69.51 (s), 47.42 (s), 35.19 (s), 14.87 (s).

2.3.5 Synthesis of PA-B-PX

PTX and succinic anhydride were first reacted in anhydrous pyridine to afford PTX-SA. PTX-SA (0.92 g, 0.96 mmol), compound 6 (0.33 g, 0.96 mmol), and DMAP (20 mg, 0.16 mmol) were dissolved in 30 mL dry CH_2Cl_2 at 0 °C followed by the addition of DCC (0.30 mg, 1.46 mmol) in 10 mL CH_2Cl_2. The reaction mixture was then warmed to room temperature and stirred overnight. After filtration, the solution was concentrated, and the crude product was purified by flash chromatography to give PA-B-PTX as a white solid (0.65 g, yield: 51.7%). Similarly, PA-H-PTX was obtained as a white solid (yield: 69.4%).

2.2.6 Synthesis of PEG-B-PTX

mPEG5k-OH (5.00 g, 1.00 mmol) was mixed with Et_3N (2 mL) in 150 mL dry THF. Methylsulfonyl chloride in 20 mL THF was then added dropwise under an argon atmosphere with magnetic stirring in an ice bath. After stirring overnight at room temperature, the mixture was filtered, and the solvent was evaporated and poured into an excess of cold ether. The precipitate was isolated, washed with ether, and dried under vacuum to obtain $mPEG_{5k}$-OMs (4.50 g, yield: 90.0%) as a white solid. ^{1}H NMR (400 MHz, $CDCl_3$) δ 4.43 – 4.31 (m, 2H), 3.78 – 3.49 (m, 458H), 3.36 (s, 3H), 3.07 (s, 3H).

$mPEG_{5k}$-OMs (4.50 g, 0.90 mmol) was dissolved in 30 mL DMF followed by the addition of NaN_3 (0.87 g, 13.4 mmol). The mixture was stirred at room temperature for 3 days and then diluted with 300 mL CH_2Cl_2. The solution was washed with brine three times and dried over anhydrous Na_2SO_4. After filtration, the solvent was evaporated, and the resulting viscous oil was precipitated in excess of cold ether. PEG_{5k}-N_3 (4.30 g. yield: 95.6%) was isolated and dried under vacuum. ^{1}H NMR (400 MHz, $CDCl_3$) δ 3.76 – 3.50 (m, 454H), 3.41 – 3.31 (m, 3H).

In a typical "click" reaction procedure, PEG_{5k}-N_3 (0.20 g, 0.04 mmol) and PA-B-PTX (76 mg, 0.06 mmol) were added to a mixture of CuBr (5.76 mg, 0.04 mmol) and PMDETA (6.92 mg, 0.04 mmol) in 2 mL of DMF. The mixture was degassed by three freeze–pump–thaw cycles, and then placed in a preheated oil bath at 40 °C. After 72 h, the reaction was quenched upon exposure to air, diluted with CH_2Cl_2, and passed through a neutral alumina column to remove the copper. The eluent was concentrated and then precipitated into a mixture of cold ethanol and ether (5:1) to remove the unreacted PA-B-PTX. The PEG-B-PTX was isolated by filtration and dried under vacuum (0.16 g, 63.8%). PEG-H-PTX was obtained similarly as a white solid (yield: 61.0%).

2.3. Preparation of PEG-B-PTX and PEG-H-PTX micelles

Prodrug micelles were prepared using a nanoprecipitation method. PEG-B-PTX (5 mg) or PEG-H-PTX (5 mg) were dissolved in 200 μL THF and added dropwise to 2 mL of deionized water with vigorous stirring. THF was removed under reduced pressure after stirring for another 30 min. The volume-averaged diameters and zeta potentials of the micelles were measured in triplicate using dynamic light scattering (DLS), and the morphology of the micelles was observed by TEM.

2.4. Critical micelle concentration (CMC) determination

The CMC of PEG-B-PTX or PEG-H-PTX was determined via the fluorescence method.[38] Briefly, Nile red (10^{-6} M, 50 μL) in CH_2Cl_2 was added into each vial. The micelle solution (5 mL) free of THF was added at a series of predetermined concentrations from 10^{-3} to 1 mg/mL. The vials were shaken overnight at 37°C in the dark at a speed of 200 rpm. The fluorescence intensity at 620 nm (579 nm excitation)

of each solution was measured by a Molecular Device SpectraMax M2e reader. The CMC was defined as the intersection of the two fitting lines of the plots of fluorescence intensity versus the prodrug concentration.

2.5. The micelles stability assessment

The PEG-B-PTX or PEG-H-PTX micelles (0.5 mM) were incubated in PBS (pH 7.4, 10 mM), cell culture medium, and 10 % FBS at 37 °C with shaking (200 rpm). The micelles' stability in response to H_2O_2 was measured in PBS (pH 7.4, 10 mM) in the presence of 200 μM H_2O_2. The micelles' size change was tracked by DLS.

2.6. *In vitro* H_2O_2 triggered PTX release

PEG-B-PTX or PEG-b-PTX micelles (1 mL, PTX equivalent concentration 1 mg/mL) were added to a dialysis tube (3500 MWCO) against 50 mL of PBS with or without H_2O_2 (200 μM) and gently shaken at 37 °C in a shaker at 150 rpm. At predetermined time intervals, 100 μL of this solution was taken out for PTX measurement by HPLC.

2.7. Cell cytotoxicity assay

The cytotoxicity of PEG-B-PTX and PEG-H-PTX was determined by 3-(4,5-dimethylthiazol-2-yl)-2,5-diphenyltetrazolium bromide (MTT) cell proliferation assay according to the manufacturer's protocol with minor changes:[39] U251 human glioma cancer cells, and MCF-7 breast cancer cells were briefly seeded into 96-well plates at a density of 5000 cells per well and incubated for 18 h followed by the addition of PMA (100 nM) and a further 6 h of incubation. After 48 h of exposure to free PTX (dissolved in DMSO), PEG-B-PTX, or PEG-H-PTX at different concentrations, 20 μL MTT (5 mg/mL) in PBS was added to each well and incubated at 37 °C for 4 h until purple precipitates were visible. The solution in each well was replaced with 100 μL of DMSO. The absorbance intensity of each well was then determined at 562/620 nm using a Molecular Devices microplate reader. Each drug concentration was tested in triplicate with three independent experiments.

2.8. Cell apoptosis measurement

For apoptosis analysis, MCF-7 cells were seeded into 12-well plates at a density of 10^4 cells per well and incubated for 18 h followed by the addition of PMA (100 nM)

with an additional 6 h of incubation. Free PTX, PEG-B-PTX, or PEG-H-PTX were added at a dose of 5 μg PTX/mL and incubated for 48 h. The medium was removed, and the cells were rinsed with PBS, detached by Trypsin, isolated, washed twice with PBS, and resuspended in PBS. Cells were treated with Annexin V-FITC Apoptosis Detection Kit (Invitrogen) and analyzed using BD FACS Calibur™ flow cytometry (Becton, Dickinson and Company, USA).

2.9. *In vivo* pharmacokinetics analysis

Taxol (prepared according to the protocol), PEG-B-PTX, or PEG-H-PTX (10 mg PTX-eq/kg) was injected intravenously into mice via the tail vein (n = 3). Blood samples (50 μL) were collected *via* the orbital venous plexus of mice at predetermined time intervals and then mixed with 0.1 M acetic acid (50 μL). The mixtures were incubated at 37 °C overnight to facilitate the release of PTX. The next day, 1 mL of methanol was added, thoroughly vortexed, ultrasonicated, and then centrifuged at 5000 rpm for 5 min. The supernatants were taken and evaporated to dryness under reduced pressure; 100 μL of acetonitrile was then added to re-dissolve the residue, and the PTX content was measured by HPLC. At the experimental endpoint, animals were sacrificed in accordance with the regulations of the Animal Care and Use Committee of Zhejiang University.

2.10. *In vivo* antitumor efficacy

Female BALB/c nude mice (6–8 weeks) were inoculated with MCF-7 cells (1×10^7 cells per mouse) via subcutaneous injection into the right flank of mice. When the inoculated tumors reached ~100 mm^3, the mice were randomized into four groups (n = 6 per group) and treated with *i.v.* injection of 0.2 mL of PBS, Taxol, PEG-H-PTX, or PEG-B-PTX at 10 mg/kg PXT-equivalent dose every two days for five times. The length (L) and width (V) of the tumors, as well as the bodyweight of mice, were monitored individually on alternate days. The tumor volume (V) was calculated using the following formula V (mm^3) = L (mm) × W (mm) ^{2} × 0.5. The mice were sacrificed on day 14 post-treatment, and the tumors were collected and weighed. The tumor inhibition rate (TIR) was calculated by the equation: TIR = (mean tumor weight of the control group − mean tumor weight of the treatment group)/mean tumor weight of

control group×100%.

2.11. Histological assay

Tumor samples were washed in PBS, fixed with 4% neutral buffered paraformaldehyde, embedded in paraffin, and cross-sectioned at a thickness of 10 μm. The sections were stained with hematoxylin-eosin (H&E, Beyotime, China) and observed under light microscopy.

2.12. Statistical analysis

Statistical analysis used Excel and Origin. Comparisons were made using a two-tailed, unpaired Student's t-test. $P < 0.05$ was considered statistically significant, and all results are expressed as mean ± standard deviation (s.d.).

3. Results and discussion

3.1. Synthesis and characterizations of PEG-B-PTX

The PEG-B-PTX was prepared as shown in **Scheme 2**. PEG-H-PTX with a benzyl ester without the benzylboronic ester was synthesized as an unresponsive counterpart for comparison. PEG-B-PTX was prepared from 2-amino-4'-bromoacetophenone hydrochloride (compound 1) in six steps. Compound 1 was first protected with a *t*-butyloxycarbonyl group followed by reduction with sodium borohydride and a Suzuki–Miyaura coupling reaction to obtain precursor 4. After deprotection in DCM/TFA, compound 5 was reacted with PA-NHS to give compound 6. Carboxylated PTX was obtained by esterification with succinic anhydride. This was reacted with compound 6 to give PA-B-PTX. Finally, PEG-B-PTX was obtained by PEG conjugation via a copper-catalyzed click reaction (**Scheme 2a**). Similarly, the control prodrug, PEG-H-PTX, was synthesized using 2-amino-1-phenylethanone hydrochloride as the starting material (**Scheme 2b)**. The ^{1}H NMR spectra (**Figs. 1a-1d**) suggested complete conjugation of PEG-N_3 and PA-B-PTX or PA-H-PTX. Similar peaks were found for PEG-B-PTX and PEG-H-PTX, except for the characteristic peak at 1.32 ppm belonging to the methyl protons of benzylboronic ester. The structures of other intermediates were also confirmed by ^{1}H and ^{13}C NMR spectra (**Figs. S1−S17**) and MALDI-TOF mass spectra

(**Fig. S18**). The molecular weights of PEG-B-PTX and PEG-H-PTX measured by MALDI-TOF were 6403.5 and 6276.8 Da, respectively, which were consistent with the theoretical values of 6404.0 and 6277.0 Da (**Figs. 1e** and 1**f**). The gel permeation chromatography (GPC) results showed that PEG-B-PTX and PEG-H-PTX are both single peaks with low polydispersity indices (PDI) of 1.06 and 1.05, respectively; these data confirm the absence of free PEG and PA-B-PTX (**Fig. 1g**). The high purity of PEG-B-PTX and PEG-H-PTX prodrugs was further confirmed by high-performance liquid chromatography (HPLC) (**Fig. S19**).

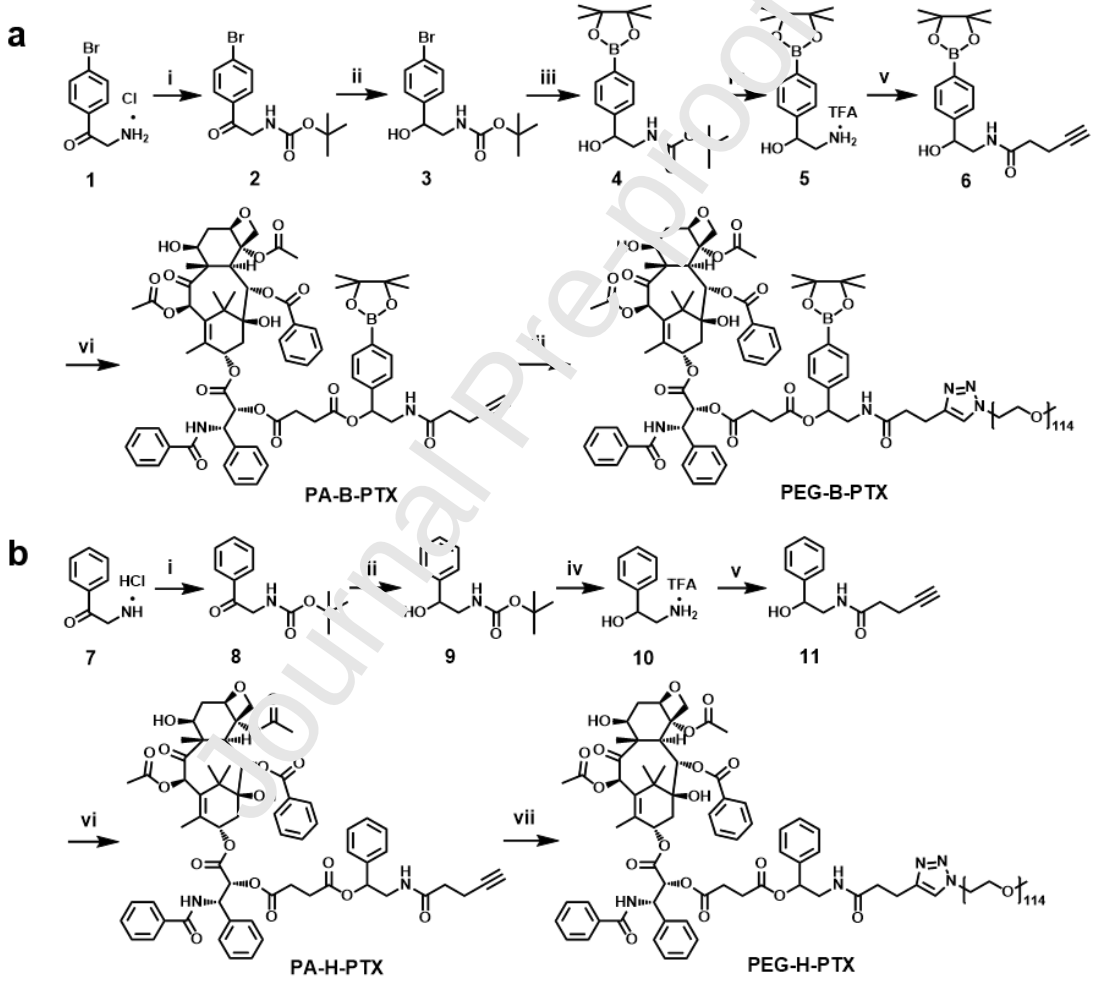

Scheme 2. Synthesis of ROS-responsive PEG-B-PTX (a) and its unresponsive control counterpart PEG-H-PTX (b). Reagents and conditions: i) $(Boc)_2O$, Et_3N, THF, 0 ºC, 30 min, 40 ºC, 2 h; ii) $NaBH_4$, MeOH, 0 ºC, 30 min; iii) Bis(pinacolato)diboron, $Pd(dppf)Cl_2{\cdot}CH_2Cl_2$, KOAc, dioxane, 90 ºC, 12h; iv) TFA/CH_2Cl_2 (1/2, v/v), RT, 6h; v) 4-pentynoic acid succinimide ester, Et_3N, CH_2Cl_2, RT, 1h; vi) PTX succinate, DCC, DMAP, CH_2Cl_2, 0 ºC, 30 min, RT, overnight; vii)

PEG-N_3, CuBr, PMDETA, DMF, 40 ºC, 72 h.

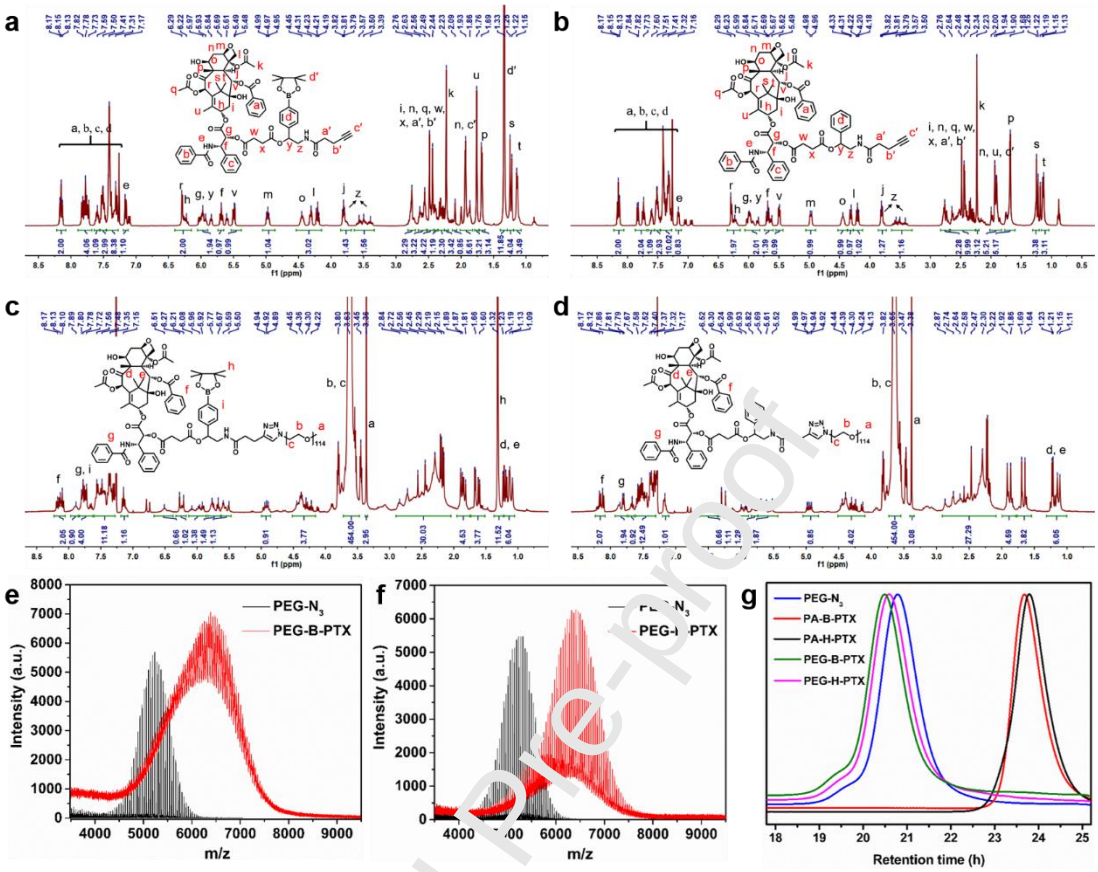

Fig. 1. Structural characterization of the prodrugs PEG-B-PTX and PEG-H-PTX. ^{1}H NMR spectra of PA-B-PTX (a), PA-H-PTX (b), PEG-B-PTX (c), and PEG-H-PTX (d) recorded in $CDCl_3$. The MALDI-TOF MS spectra of PEG-B-PTX (e) and PEG-H-PTX (f). GPC traces obtained for PEG-N_3, PA-B-PTX, PA-H-PTX, PEG-B-PTX, and PEG-H-PTX (DMF, 50°C, 0.8 mL/min) (g).

The PTX contents of PEG-B-PTX and PEG-H-PTX were 13.3% and 13.6% by weight, respectively, as determined by HPLC. These amphiphilic prodrugs self-assembled into micelles with similar sizes around 50 nm in diameter as determined by DLS and confirmed by TEM **(Fig. 2a)**. TEM images showed that the nanoparticles were spherical and had a dark core indicating a micellar rather than vesicular structure. The two prodrugs also had a similar critical micelle concentration of around 30 μg/mL (**Fig. S20**). The low CMCs ensures the *in vitro* and *in vivo* stability of their micelles. Notably, both PEG-B-PTX and PEG-H-PTX nanoparticle solutions were stable for several months at 4 °C.

3.2. ROS-responsive PTX release

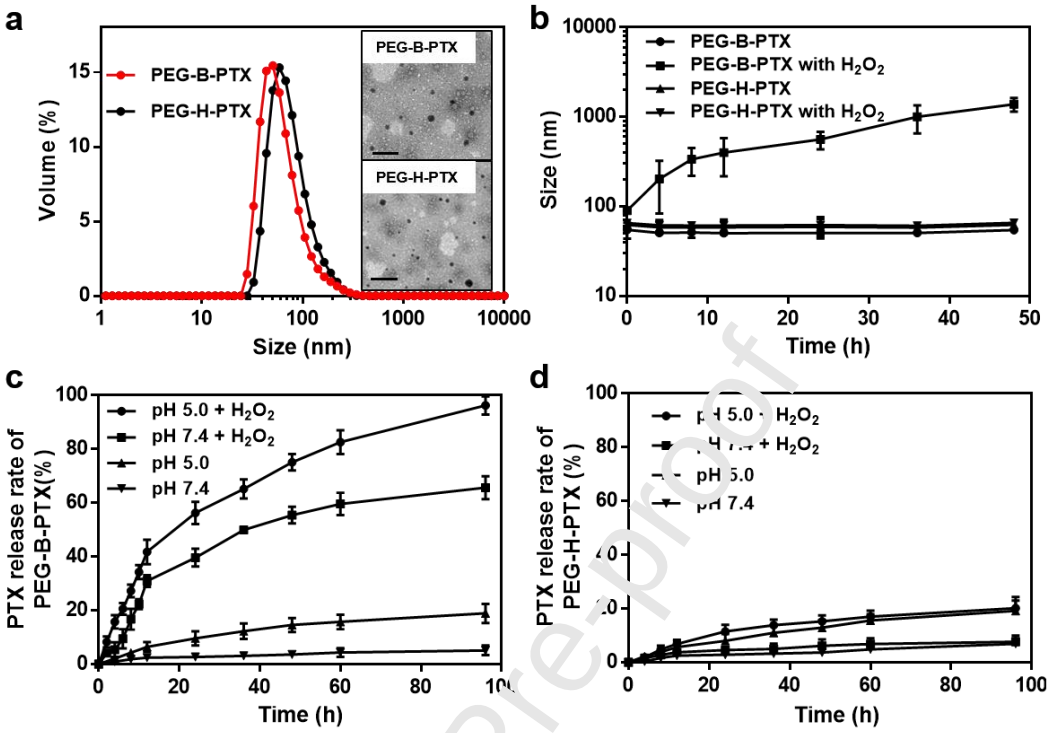

Fig. 2. Micelle formation and drug release of PEG-B-PTX and PEG-H-PTX prodrugs. (a) Size distribution patterns of PEG-B-PTX and PEG-H-PTX micelles determined by DLS and their morphologies observed by TEM (inserted, scale bar = 200 nm); the prodrugs were dissolved in water at a concentration of 0.5 mM. (b) The time-dependent size changes of PEG-B-PTX and PEG-H-PTX micelles (0.5 mM) with or without 200 μM H_2O_2 at 37 °C determined by DLS measurement. PTX release profiles of PEG-B-PTX (c) and PEG-H-PTX (d) with or without 200 μM H_2O_2 at pH 7.4 and 5.0.

The stability of micelles in 200 μM H_2O_2 in PBS (pH 7.4, 10 mM) was tracked by DLS. The PEG-B-PTX micelles showed robust stability in the absence of H_2O_2, but they gradually aggregated after treatment with H_2O_2; the sizes increased from 50 nm to 400 nm over 10 h and reached over 1 μm after 48 h (**Fig. 2b**). The formation of aggregates was probably due to the oxidative cleavage of the intermediate phenylboronic ester linkage resulting in shedding of the PEG corona and aggregation of the released hydrophobic drugs (**Scheme 1**). In contrast, no size change of

PEG-H-PTX micelles was observed in either the presence or absence of H_2O_2.

The corresponding PTX release from PEG-B-PTX micelles was investigated using dialysis bags in PBS under different pH and redox conditions to mimic different physiological environments. PEG-B-PTX and PEG-H-PTX micelles were both very stable and free of burst release with only 5% PTX release after 96 h in PBS at pH 7.4 without H_2O_2 (**Fig. 2c** and **d)**. The acidic condition (pH 5.0) slightly promoted PTX release from both micelles due to the acid-catalyzed hydrolysis of the ester bond [40]. As expected, H_2O_2 did not promote the PTX release from PEG-H-PTX micelles but did dramatically accelerate the PEG-B-PTX release rate from 2% to 31% in 12 h and 65% in 96 h upon addition of 200 μM H_2O_2 at pH 7.4. Notably, the PTX release was much faster if the micelles were incubated at pH 5.0 with H_2O_2 because of the stronger oxidation potential of H_2O_2 in acidic solution [41]. Thus, the PEG-B-PTX would remain stable in blood but display a fast PTX release in tumor tissues—especially in the acidic tumor interstitium and lysosomes [42].

The ROS-trigged drug release of PEG-B-PTX may take place over two steps: (i) oxidation of phenylboronic ester and subsequent 1,4-elimination [43] and (ii) hydrolysis of succinate ester and release of PTX molecule. PEG-B-PTX was very stable under normal physiological environments, and the esters could not be hydrolyzed due to its steric hindrance and hydrophobicity. However, after the boronic ester was oxidized, the resulting phenolate would undergo a spontaneous 1,4-elimination to break the PEG-B-PTX conjugate with subsequent release of the PTX succinate. After the removal of the hydrophobic phenylboronic acid pinacol ester, the ester bond conjugated with PTX was further hydrolyzed due to its decreased steric hindrance and the nearby hydrophilic environment. Thus, free PTX molecules were successfully released.

3.3. *In vitro* cytotoxicity

The cytotoxicity of these two prodrugs was compared on U251 human glioma cancer cells and MCF-7 human breast cancer cells. Tumor cells are characterized by high levels of ROS, which are responsive to various tumor microenvironments such as proliferation-induced hypoxia and reoxygenation [44]. To mimic the high ROS

levels of tumor cells *in vivo*, an intracellular ROS stimulator phorbol-12-myristate-13-acetate (PMA) [45] was preincubated with cells to elevate the intracellular ROS level. The intracellular ROS was visualized by confocal laser scanning microscopy (CLSM) using 2′,7′-dichlorodihydrofluorescein diacetate (H_2DCFDA)—this probe is non-fluorescent but is oxidized to 2′,7′-dichlorodihydrofluorescein (DCF) upon oxidation by the intracellular ROS [46]. The MCF-7 cells cultured with H_2DCFDA (10 μM) showed low green fluorescence. Strong green fluorescence was observed when cells were pretreated with PMA (100 nM) for 6 h, and the fluorescence declined to the control group level 12 h after the treatment (**Fig. 3a**).

The PEG-B-PTX and PEG-H-PTX showed comparable cytotoxicity without PMA stimulation with IC_{50} values of 3.87 μg/mL and 4.86 μg/mL on U251 cells, and 13.7 μg/mL and 9.47 μg/mL on MCF-7 cells, respectively (**Figs. 3b** and **3c**). With PMA stimulation, the cytotoxicity of PEG-B-PTX was greatly enhanced: The IC50 value was reduced by 11- and 14-folds on U251 and MCF-7 cells, respectively. Notably, the cytotoxicity of PEG-B-PTX (IC_{50} = 0.35 μg/mL) was even higher than PTX (IC_{50} = 1.08 μg/mL) upon PMA stimulation on U251 cell line. The PEGylated prodrug reversed the drug resistance of U251 cells, efficiently entering the cells, and PMA induced ROS elevation, triggering the fast release of PTX and enhancing the cytotoxicity. PMA stimulation has no significant effect on the cytotoxicity of PEG-H-PTX in either cell lines **(Fig. 3b** and 3**c**). We further studied the cell apoptosis-inducing capability of both prodrugs by Annexin V-PI assay. The percentage of cells in late apoptosis (both Annexin and PI-positive) was similar via the treatment of PEG-B-PTX (14.38%) and PEG-H-PTX (13.17%) on cells without PMA stimulation. However, once cells were pretreated with PMA, the percentage of cells in late apoptosis increased to 30.75% after the treatment of PEG-B-PTX. This was comparable to values in cells treated with free PTX (32.80%). In comparison, the apoptosis-inducing ability of the unresponsive PEG-H-PTX was only slightly affected by the elevated intracellular ROS level (18.68% *vs.* 13.17%). These findings

confirmed the crucial role of the ROS-responsive linker in the prodrug. The ROS-triggered release of PTX-SA and its quick hydrolysis into free PTX in the cell generated high cytotoxicity [47].

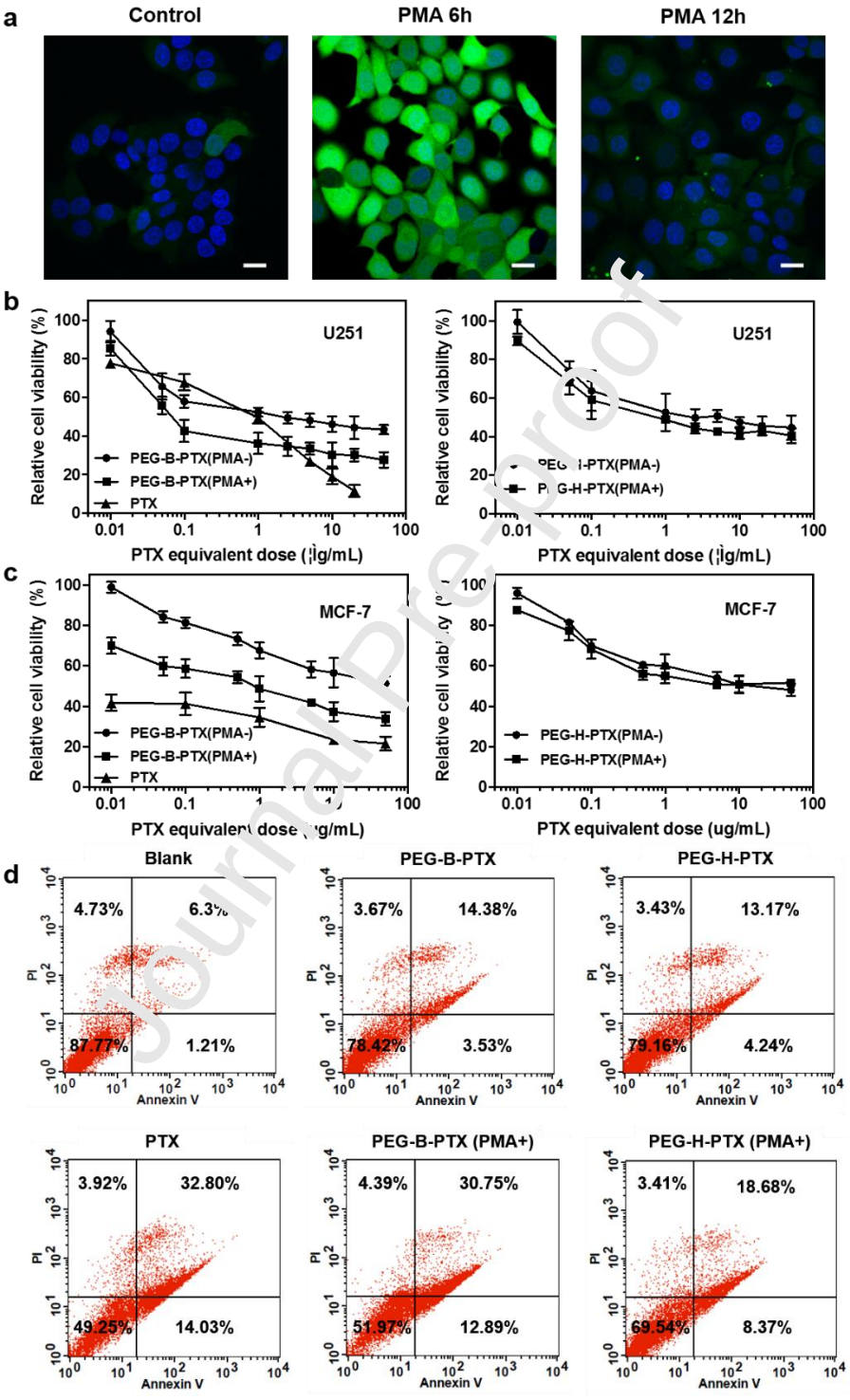

Fig. 3. ROS-dependent cell cytotoxicity. (a) Confocal microscopy images of intracellular ROS generation in MCF-7 cells with or without 200 nM PMA for 6 or 12 h. All scale bars are 20 μm. Cell nuclei are stained by Hoechst 33342 and expressed as

blue. 2′,7′-Dichlorodihydrofluorescein (DCF)-induced by ROS is expressed as green. (b, c) Effect of PMA-pretreatment on the cell cytotoxicity of PEG-B-PTX and PEG-H-PTX to U251 cells (b) and MCF-7 cells (c). The cells were pretreated with PMA (200 nM) for 6 h before the addition of the prodrug and free PTX. (d) The apoptosis of MCF-7 cells was determined by Annexin V/propidium iodide double staining. Cells were treated with PEG-B-PTX or PEG-H-PTX (PTX equivalent dose 5 μg/mL) for 48 h.

3.4. Pharmacokinetics

The *in vivo* stealth property of PEG-B-PTX and PEG-H-PTX was subsequently estimated by monitoring their blood clearance kinetics. Blood samples were collected *via* the orbital venous plexus of mice at different intervals after a single intravenous injection of PEG-B (H)-PTX or Taxol (PTX equivalent dose 10 mg/kg, n = 3). The PTX content in plasma at different time intervals was determined by HPLC (**Fig. 4**). Taxol was quickly cleared, and only 0.1% of the injected dose remained after 6 h. In contrast, both PEG-B-PTX and PEG-H-PTX were slowly cleared; more than 10% of the injected dose remained after 6 h. The blood clearance half-life ($T_{1/2}$) and area-under-curve (AUC) values of the formulations are listed in Table 1. The PEG-B-PTX and PEG-H-PTX micelles exhibited superior pharmacokinetics to Taxol with ~9.4 (10.4)-fold longer $T_{1/2\beta}$ and 4.8 (5.6)-fold larger AUC (P<0.05). Hence, the PEG-B-PTX and PEG-H-PTX micelles had more favorable pharmacokinetics to extravasate from the leaky tumor vasculature and can accumulate in tumor tissue [48].

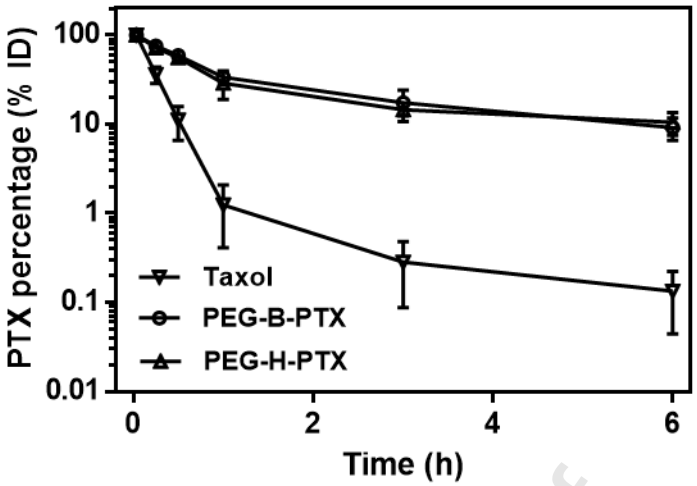

Fig. 4. Blood clearance kinetics of PTX after a single injection of PEG-B-PTX, PEG-H-PTX, and Taxol at a PTX equivalent dose of 10 mg/kg (n = 3).

Table 1. Blood half-life and area under the curve for different formulations of ICR mice at a PTX-equivalent dose of 10 mg/kg.

Parameter	Unit	PEG-B-PTX	PEG-H-PTX	Taxol
$T_{1/2}$ alpha	h	0.41 ± 0.03	0.41 ± 0.10	0.10 ± 0.08
$T_{1/2}$ beta	h	4.93 ± 1.61	5.44 ± 2.06	0.18 ± 0.05
$AUC_{0\sim t}$	$\mu g\ mL^{-1}\ h^{-1}$	153.73 ± 29.20	140.11 ± 16.73	29.63 ± 1.80

$T_{1/2}$ alpha: the half-life of the distribution phase. $T_{1/2}$ beta: the half-life of elimination phases. Data are depicted as mean ± SD. Statistical significance: $^*P<0.05$.

3.5. *In vivo* antitumor efficacy

The *in vivo* antitumor activity of PEG-B-PTX micelles was compared with PEG-H-PTX, Taxol, and PBS using an MCF-7 xenograft tumor model (**Figs. 5a-5d**). The mice were randomly divided into four groups (n = 6) when the tumors reached about 100 mm^3; treatments were intravenously administered every two days for five times. The mice were sacrificed one week after the last treatment, and the tumors were extracted and weighted. Versus PBS, all treatments of PTX formulations led to significant tumor growth inhibition. PEG-B-PTX exhibited the best antitumor activity with a tumor inhibition rate of 89.4%, which is attributed to its favorable pharmacokinetics and tumor-specific drug release. Unexpectedly, PEG-H-PTX

showed an even lower tumor inhibition rate (57.6%) than Taxol (68.5%, $P < 0.05$), although PEG-H-PTX also has favorable pharmacokinetics. This result further highlights the importance of the drug release profiles in affecting the antitumor activity. The strong tumor inhibition capability of PEG-B-PTX was supported by the histological analysis of tumor tissues—more apoptotic cells were found in tumors treated with PEG-B-PTX than those treated with PEG-H-PTX or Taxol (**Fig. 5e**). Moreover, no significant body weight loss was observed in the mice treated with either PEG-B-PTX or PEG-H-PTX, but the mice treated with Taxol showed severe body weight loss. The low toxicity of PEG-B-PTX and PEG-H-PTX prodrugs is attributed to their improved pharmacokinetic profiles.

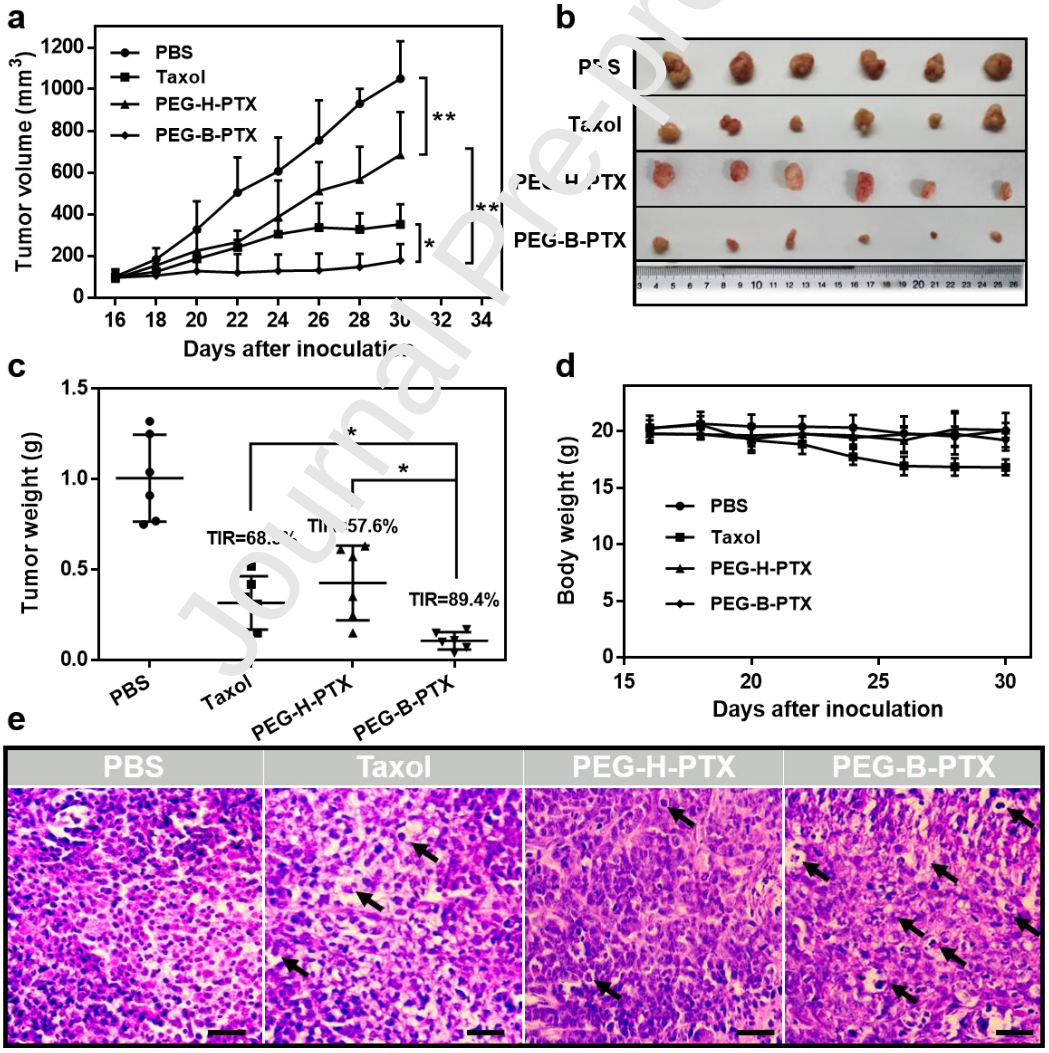

Fig. 5. *In vivo* antitumor activity. (a) The MCF-7 tumor volume changes in mice treated with PBS, PEG-B-PTX, PEG-H-PTX, or Taxol (PTX-equivalent dose 10

mg/kg) with five replicate doses. (b) The average tumor weight of each group at the end of the experiment. (c) The body weight variation of tumor-bearing mice during the treatment (d) Images of the MCF-7 xenograft tumors of the mice at the end of the experiment. (e) Representative histological features of the tumors 7 days after the last treatment. Tissue paraffin sections were 10-μm thick. The tumor sections were stained with hematoxylin–eosin and examined by light microscopy. Scale bars = 50 μm. Error bars indicate s.d. (n = 6). *P < 0.05, **P < 0.01 (two-tailed Student's t-test).

4. Conclusion

We developed a novel ROS-responsive prodrug, PEG-B-PTX, by incorporating a benzylboronic ester linker between PEG and PTX. The PEG-B-PTX prodrug has a high drug loading content and can self-assemble into stable ~50 nm micelles. The micelles are free of PTX release in the normal physiological environment but quickly release PTX in tumor sites after ROS oxidation. As a result, the PEG-B-PTX prodrug shows a more potent antitumor activity than an unresponsive counterpart PEG-H-PTX prodrug and the clinical first-line drug Taxol. Moreover, the PEG-B-PTX prodrug exhibits reduced systemic toxicity versus Taxol. Thus, this ROS-responsive prodrug design is promising for cancer drug delivery. Importantly, this strategy may not be limited to the delivery of PTX but can also be used to deliver other chemotherapeutic drugs, bioactive peptides, and proteins.

Acknowledgements

We thank the National Natural Science Foundation of China (51833008, 21875211, 81672478, U1501243, and 51603181), the National Key Research and Development Program of China (2016YFA0200301), and the Fundamental Research Funds for the Central Universities of China (2019FZA4020).

Credit Author Statement

Chengyuan Dong, Quan Zhou, and Jiajia Xiang: Investigation, Methodology, Formal analysis, Writing - Original Draft. **Fusheng Liu:** Supervision, Visualization, Funding acquisition. **Zhuxian Zhou and Youqing Shen:** Writing -

Review & Editing, Supervision, Funding acquisition

Supplementary data

Supplementary material

References

[1] J. Sandercock, M. Parmar, V. Torri, W. Qian, First-line treatment for advanced ovarian cancer: paclitaxel, platinum and the evidence, Br. J. Cancer, 87 (2002) 815-824.
[2] J. Crown, M. O'leary, The taxanes: an update, Lancet, 355 (2000) 1176-1178.
[3] F.H. Wang, M. Porter, A. Konstantopoulos, P.C. Zhang, H.G. Cui, Preclinical development of drug delivery systems for paclitaxel-based cancer chemotherapy, J. Control. Release, 267 (2017) 100-118.
[4] Y.J. Zhang, Z.Y. Guo, Z.L. Cao, W.X. Zhou, Y. Zhang, Q.J. Chen, Y.F. Lu, X.L. Chen, Q. Guo, C. Li, D.H. Liang, T. Sun, C. Jiang, Endogenous albumin-mediated delivery of redox-responsive paclitaxel-loaded micelles for targeted cancer therapy, Biomaterials, 183 (2018) 243-257.
[5] J. Xiang, B. Wu, Z. Zhou, S. Hu, Y. Piao, Q. Zhou, G. Wang, J. Tang, X. Liu, Y. Shen, Synthesis and evaluation of a paclitaxel-binding polymeric micelle for efficient breast cancer therapy, Sci. China Life Sci., 61 (2018) 436-447.
[6] J. Huang, B. Wu, Z. Zhou, S. Hu, F. Xu, Y. Piao, H. Zheng, J. Tang, X. Liu, Y. Shen, Drug-binding albumins forming stabilized nanoparticles for efficient anticancer therapy, Nanomed. Nanotechnol. Biol. Med., 21 (2019) 102058.
[7] R.W. Chakroun, F.H. Wang, R. Lin, Y. Wang, H. Su, D. Pompa, H.G. Cui, Fine-Tuning the Linear Release Rate of Paclitaxel-Bearing Supramolecular Filament Hydrogels through Molecular Engineering, ACS Nano, 13 (2019) 7780-7790.
[8] E. Miele, G.P. Spinelli, E. Miele, F. Tomao, S. Tomao, Albumin-bound formulation of paclitaxel (Abraxane (R) ABI-007) in the treatment of breast cancer, Int. J. Nanomed., 4 (2009) 99-105.
[9] I.H. Park, J.H. Sohn, S.B. Kim, K.S. Lee, J.S. Chung, S.H. Lee, T.Y. Kim, K.H. Jung, E.K. Cho, Y.S. Kim, H.S. Song, J.H. Seo, H.M. Ryoo, S.A. Lee, S.Y. Yoon, C.S. Kim, Y.T. Kim, S.Y. Kim, M.R. Jin, J. Ro, An open-label, randomized, parallel, phase III trial evaluating the efficacy and safety of polymeric micelle-formulated paclitaxel compared to conventional cremophor EL-based paclitaxel for recurrent or metastatic HER2-negative breast cancer, Cancer Res. Treat., 49 (2017) 569-577.
[10] Z. Feng, G. Zhao, L. Yu, D. Gough, S.B. Howell, Preclinical efficacy studies of a novel nanoparticle-based formulation of paclitaxel that out-performs Abraxane, Cancer Chemother. Pharmacol., 65 (2010) 923-930.
[11] D.L. Stirland, J.W. Nichols, S. Miura, Y.H. Bae, Mind the gap: A survey of how cancer drug carriers are susceptible to the gap between research and practice, J. Control. Release, 172 (2013) 1045-1064.
[12] Q. Sun, Z. Zhou, N. Qiu, Y. Shen, Rational Design of Cancer Nanomedicine:

Nanoproperty Integration and Synchronization, Adv. Mater., 29 (2017) 1606628.
[13] S. Mura, J. Nicolas, P. Couvreur, Stimuli-responsive nanocarriers for drug delivery, Nat. Mater., 12 (2013) 991-1003.
[14] J. Wang, X. Sun, W. Mao, W. Sun, J. Tang, M. Sui, Y. Shen, Z. Gu, Tumor redox heterogeneity-responsive prodrug nanocapsules for cancer chemotherapy, Adv. Mater., 25 (2013) 3670-3676.
[15] Z. Zhou, X. Ma, C.J. Murphy, E. Jin, Q. Sun, Y. Shen, E.A. Van Kirk, W.J. Murdoch, Molecularly precise dendrimer-drug conjugates with tunable drug release for cancer therapy, Angew. Chem. Int. Ed., 53 (2014) 10949-10955.
[16] J. Wang, S. Hu, W. Mao, J. Xiang, Z. Zhou, X. Liu, J. Tang, Y. Shen, Assemblies of Peptide-Cytotoxin Conjugates for Tumor-Homing Chemotherapy, Adv. Funct. Mater., 29 (2019) 1807446.
[17] Q. Zhou, S. Shao, J. Wang, C.H. Xu, J. Xiang, Y. Piao, Z. Zhou, Q.S. Yu, J. Tang, X. Liu, Z. Gan, R. Mo, Z. Gu, Y. Shen, Enzyme-activatable polymer-drug conjugate augments tumour penetration and treatment efficacy, Nat. Nanotechnol., 14 (2019) 799-811.
[18] B.L. Sui, C. Cheng, M.M. Wang, E. Hopkins, P.S. Xu, Heterotargeted Nanococktail with Traceless Linkers for Eradicating Cancer, Adv. Funct. Mater., 29 (2019) 1906433.
[19] J. Bhattacharyya, J.J. Bellucci, I. Weitzhandler, J.R. McDaniel, I. Spasojevic, X.H. Li, C.C. Lin, J.T.A. Chi, A. Chilkoti, A paclitaxel-loaded recombinant polypeptide nanoparticle outperforms Abraxane in multiple murine cancer models, Nat. Commun., 6 (2015) 7939.
[20] F.W. Zhang, S.Y. Zhang, S.F. Pollack, R.C. Li, A.M. Gonzalez, J.W. Fan, J. Zou, S.E. Leininger, A. Pavia-Sanders, R. Johnson, L.D. Nelson, J.E. Raymond, M. Elsabahy, D.M.P. Hughes, M.W. Lenox, T.P. Gustafson, K.L. Wooley, Improving paclitaxel delivery: In vitro and in vivo characterization of PEGylated polyphosphoester-based nanocarriers, J. Am. Chem. Soc., 137 (2015) 2056-2066.
[21] D.Q. Chen, G.Q. Zhang, R.M. Li, M.R. Guan, X.Y. Wang, T.J. Zou, Y. Zhang, C.R. Wang, C.Y. Shu, F. Hong, L.J. Wan, Biodegradable, hydrogen peroxide, and glutathione dual responsive nanoparticles for potential programmable paclitaxel release, J. Am. Chem. Soc., 140 (2018) 7373-7376.
[22] X.D. Ma, E. Ozliseli, Y.Z. Zhang, G.Q. Pan, D.Q. Wang, H.B. Zhang, Fabrication of redox-responsive doxorubicin and paclitaxel prodrug nanoparticles with microfluidics for selective cancer therapy, Biomater. Sci., 7 (2019) 634-644.
[23] W. Zhang, X. Hu, Q. Shen, D. Xing, Mitochondria-specific drug release and reactive oxygen species burst induced by polyprodrug nanoreactors can enhance chemotherapy, Nat. Commun., 10 (2019) 1704.
[24] R. Lin, A.G. Cheetham, P.C. Zhang, Y.A. Lin, H.G. Cui, Supramolecular filaments containing a fixed 41% paclitaxel loading, Chem. Commun., 49 (2013) 4968-4970.
[25] X.L. Hu, G.H. Liu, Y. Li, X.R. Wang, S.Y. Liu, Cell-penetrating hyperbranched polyprodrug amphiphiles for synergistic reductive milieu-triggered drug release and enhanced magnetic resonance signals, J. Am. Chem. Soc., 137 (2015) 362-368.

[26] C.E. Callmann, C.V. Barback, M.P. Thompson, D.J. Hall, R.F. Mattrey, N.C. Gianneschi, Therapeutic enzyme-responsive nanoparticles for targeted delivery and accumulation in tumors, Adv. Mater., 27 (2015) 4611-4615.
[27] Y. Shen, E. Jin, B. Zhang, C.J. Murphy, M. Sui, J. Zhao, J. Wang, J. Tang, M. Fan, E. Van Kirk, W.J. Murdoch, Prodrugs forming high drug loading multifunctional nanocapsules for intracellular cancer drug delivery, J. Am. Chem. Soc., 132 (2010) 4259-4265.
[28] X. Hu, S. Zhai, G. Liu, D. Xing, H. Liang, S. Liu, Concurrent drug unplugging and permeabilization of polyprodrug-gated crosslinked vesicles for cancer combination chemotherapy, Adv. Mater., 30 (2018) 1706307.
[29] L. Bildstein, C. Dubernet, P. Couvreur, Prodrug-based intracellular delivery of anticancer agents, Adv. Drug Deliv. Rev., 63 (2011) 3-23.
[30] J.J. Cheng, R. Tong, Paclitaxel-initiated, controlled polymerization of lactide for the formulation of polymeric nanoparticulate delivery vehicles, Angew. Chem. Int. Ed., 47 (2008) 4830-4834.
[31] T.P. Szatrowski, C.F. Nathan, Production of large amounts of hydrogen peroxide by human tumor cells, Cancer Res., 51 (1991) 794-798.
[32] D. Trachootham, J. Alexandre, P. Huang, Targeting cancer cells by ROS-mediated mechanisms: a radical therapeutic approach?, Nat. Rev. Drug Discovery, 8 (2009) 579-591.
[33] J. Xiang, X. Liu, Z. Zhou, D. Zhu, Q. Zhou, Y. Piao, L. Jiang, J. Tang, X. Liu, Y. Shen, Reactive Oxygen Species (ROS)-Responsive Charge-Switchable Nanocarriers for Gene Therapy of Metastatic Cancer, ACS Appl. Mater. Inter., 10 (2018) 43352-43362.
[34] D. Zhu, H. Yan, X. Liu, J. Xiang, Z. Zhou, J. Tang, X. Liu, Y. Shen, Intracellularly Disintegratable Polysulfoniums for Efficient Gene Delivery, Adv. Funct. Mater., 27 (2017) 1606826.
[35] M. Ye, Y. Han, J. Tang, Y. Piao, X. Liu, Z. Zhou, J. Gao, J. Rao, Y. Shen, A tumor-specific cascade amplification drug release nanoparticle for overcoming multidrug resistance in cancers, Adv. Mater., (2017) 1702342.
[36] J. Noh, B. Kwon, E. Han, M. Park, W. Yang, W. Cho, W. Yoo, G. Khang, D. Lee, Amplification of oxidative stress by a dual stimuli-responsive hybrid drug enhances cancer cell death, Nat. Commun., 6 (2015) 6907.
[37] J. Li, A. Dirisala, Z. Ge, Y. Wang, W. Yin, W. Ke, K. Toh, J. Xie, Y. Matsumoto, Y. Anraku, Therapeutic vesicular nanoreactors with tumor- specific activation and self- destruction for synergistic tumor ablation, Angew. Chem. Int. Ed., 129 (2017) 14213-14218.
[38] Z. Zhou, X. Ma, E. Jin, J. Tang, M. Sui, Y. Shen, E.A. Van Kirk, W.J. Murdoch, M. Radosz, Linear-dendritic drug conjugates forming long-circulating nanorods for cancer-drug delivery, Biomaterials, 34 (2013) 5722-5735.
[39] Z. Zhou, Y. Piao, L. Hao, G. Wang, Z. Zhou, Y. Shen, Acidity-responsive shell-sheddable camptothecin-based nanofibers for carrier-free cancer drug delivery, Nanoscale, 11 (2019) 15907-15916.
[40] Z. Zhang, L. Mei, S.-S. Feng, Paclitaxel drug delivery systems, Expert Opin.

Drug Delivery, 10 (2013) 325-340.
[41] X. Liu, J.J. Xiang, D.C. Zhu, L.M. Jiang, Z.X. Zhou, J.B. Tang, X.R. Liu, Y.Z. Huang, Y.Q. Shen, Fusogenic reactive oxygen species triggered charge-reversal vector for effective gene delivery, Adv. Mater., 28 (2016) 1743-1752.
[42] E.L. Jin, B. Zhang, X.R. Sun, Z.X. Zhou, X.P. Ma, Q.H. Sun, J.B. Tang, Y.Q. Shen, E.V. Kirk, W.J. Murdoch, M. Radosz, Acid-active cell-penetrating peptides for in vivo tumor-targeted drug delivery, J. Am. Chem. Soc., 135 (2012) 933-940.
[43] C. de Gracia Lux, S. Joshi-Barr, T. Nguyen, E. Mahmoud, E. Schopf, N. Fomina, A. Almutairi, Biocompatible polymeric nanoparticles degrade and release cargo in response to biologically relevant levels of hydrogen peroxide, J. Am. Chem. Soc., 134 (2012) 15758-15764.
[44] S. Prasad, S.C. Gupta, A.K. Tyagi, Reactive oxygen species (ROS) and cancer: Role of antioxidative nutraceuticals, Cancer Lett., 387 (2017) 95-105.
[45] Z. Deng, Y. Qian, Y. Yu, G. Liu, J. Hu, G. Zhang, S. Liu, Engineering intracellular delivery nanocarriers and nanoreactors from oxidation-responsive polymersomes via synchronized bilayer cross-linking and permeabilizing inside live cells, J. Am. Chem. Soc., 138 (2016) 10452.
[46] Y. Yuan, C.J. Zhang, B. Liu, A photoactivatable AIE polymer for light-controlled gene delivery: concurrent endo/lysosomal escape and DNA unpacking, Angew. Chem. Int. Ed., 54 (2015) 11419-11423.
[47] H.M. Deutsch, J.A. Glinski, M. Hernandez, R.D. Haugwitz, V.L. Narayanan, M. Suffness, L.H. Zalkow, Synthesis of congeners and prodrugs. 3. Water-soluble prodrugs of taxol with potent antitumor activity J. Med. Chem., 32 (1989) 788-792.
[48] Z. Zhou, X. Liu, D. Zhu, Y. Wang, Z. Zhang, X. Zhou, N. Qiu, X. Chen, Y. Shen, Nonviral Cancer Gene Therapy: Delivery Cascade and Vector Nanoproperty Integration, Adv. Drug Deliv. Rev., 115 (2017) 115-154.

Schemes, Figures and Table

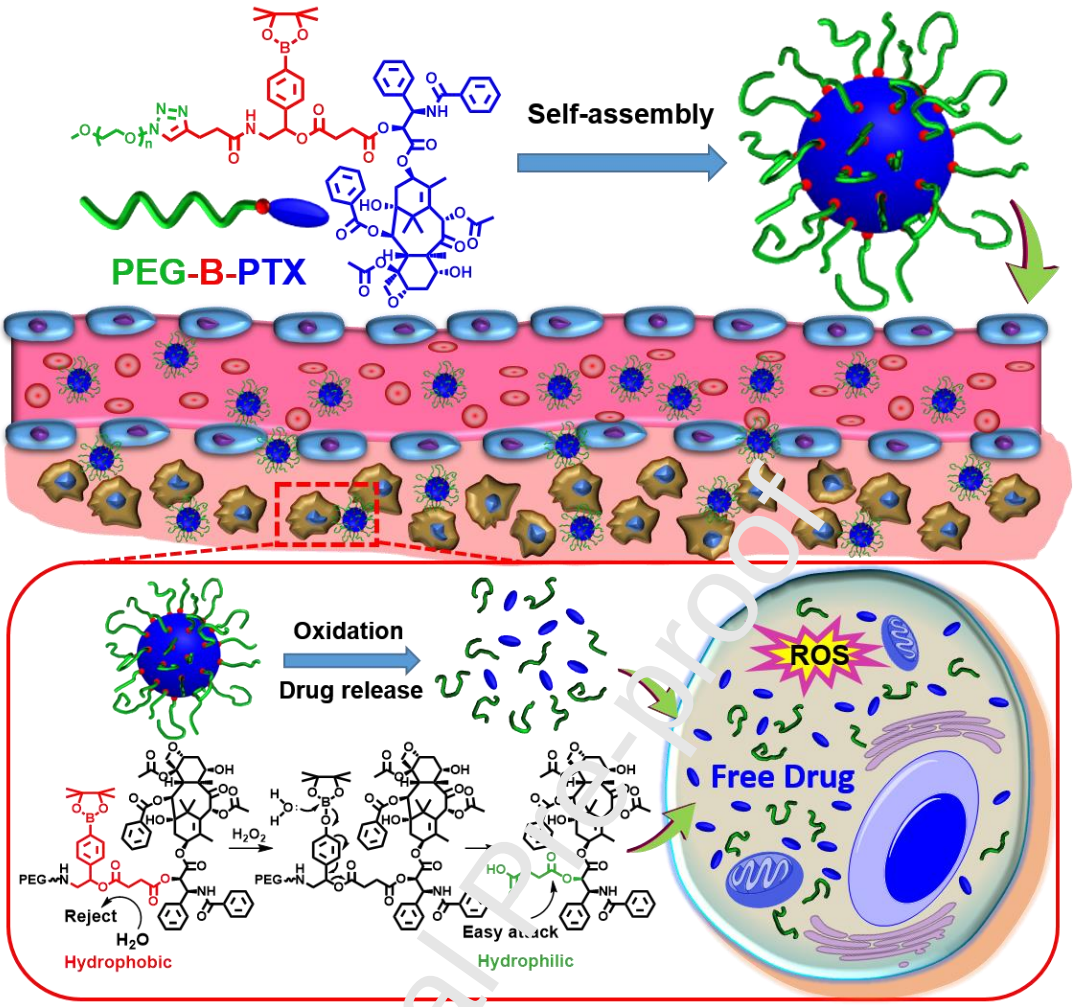

Scheme 1. The chemical structure of the PTX prodrug, PEG-B-PTX, and it's self-assembly into prodrug micelles for the tumor ROS-triggered drug release.

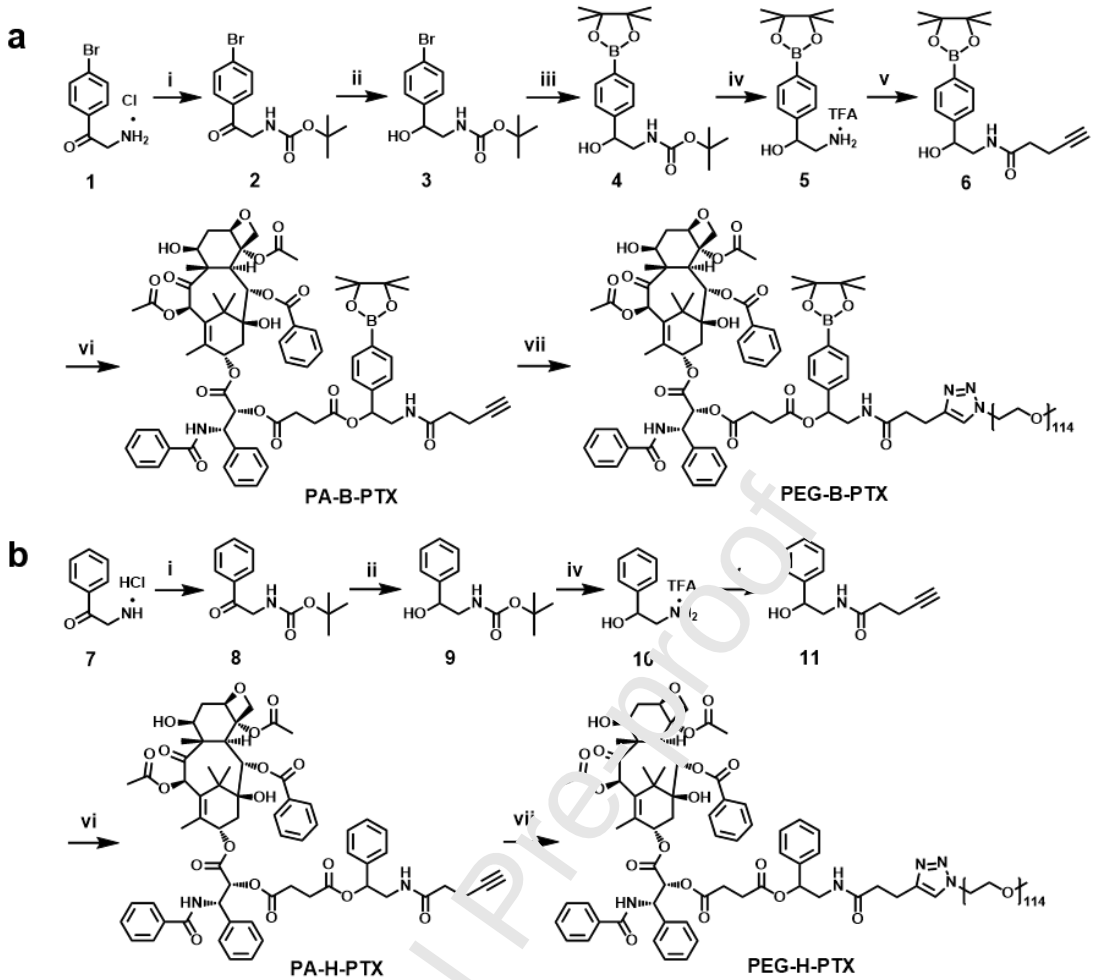

Scheme 2. Synthesis of ROS-responsive PEG-B-PTX (a) and its unresponsive control counterpart PEG-H-PTX (b). Reagents and conditions: i) $(Boc)_2O$, Et_3N, THF, 0 ºC, 30 min, 40 ºC, 2 h; ii) $NaBH_4$, MeOH, 0 ºC, 30 min; iii) Bis(pinacolato)diboron, $Pd(dppf)Cl_2{\cdot}CH_2Cl_2$, KOAc, dioxane, 90 ºC, 12h; iv) TFA/CH_2Cl_2 (1/2, v/v), RT, 6h; v) 4-pentynoic acid succinimide ester, Et_3N, CH_2Cl_2, RT, 1h; vi) PTX succinate, DCC, DMAP, CH_2Cl_2, 0 ºC, 30 min, RT, overnight; vii) PEG-N_3, CuBr, PMDETA, DMF, 40 ºC, 72 h.

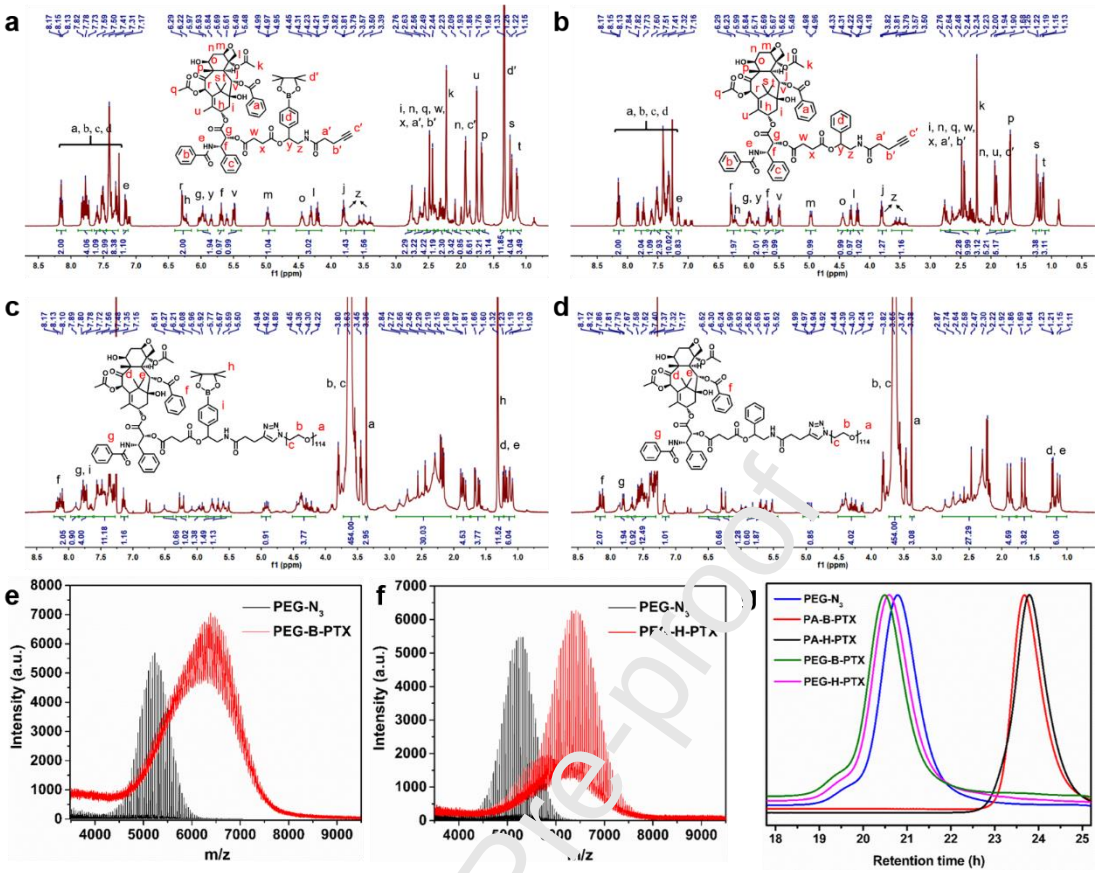

Fig. 1. Structural characterization of the prodrugs PEG-B-PTX and PEG-H-PTX. ^{1}H NMR spectra of PA-B-PTX (a), PA-H-PTX (b), PEG-B-PTX (c), and PEG-H-PTX (d) recorded in $CDCl_3$. The MALDI-TOF MS spectra of PEG-B-PTX (e) and PEG-H-PTX (f). GPC traces obtained for PEG-N_3, PA-B-PTX, PA-H-PTX, PEG-B-PTX, and PEG-H-PTX (DMF, 50°C, 0.8 mL/min) (g).

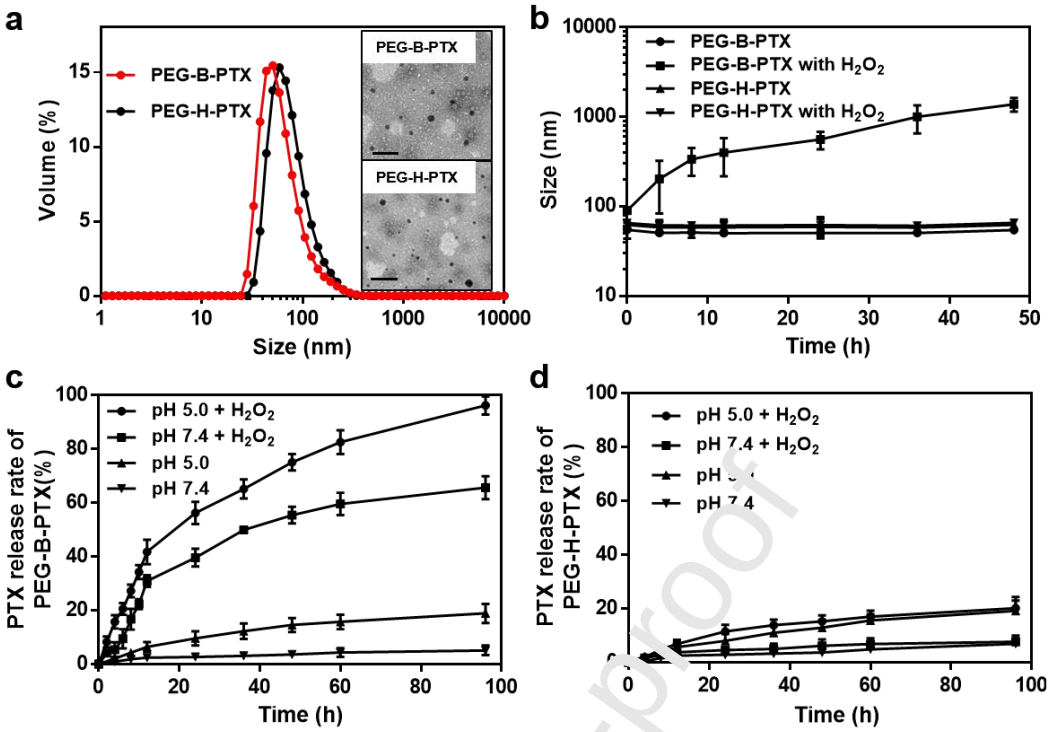

Fig. 2. Micelle formation and drug release of PEG-B-PTX and PEG-H-PTX prodrugs. (a) Size distribution patterns of PEG-B-PTX and PEG-H-PTX micelles determined by DLS and their morphologies observed by TEM (inserted, scale bar = 200 nm); the prodrugs were dissolved in water at a concentration of 0.5 mM. (b) The time-dependent size changes of PEG-B-PTX and PEG-H-PTX micelles (0.5 mM) with or without 200 μM H_2O_2 at 37 °C determined by DLS measurement. PTX release profiles of PEG-B-PTX (c) and PEG-H-PTX (d) with or without 200 μM H_2O_2 at pH 7.4 and 5.0.

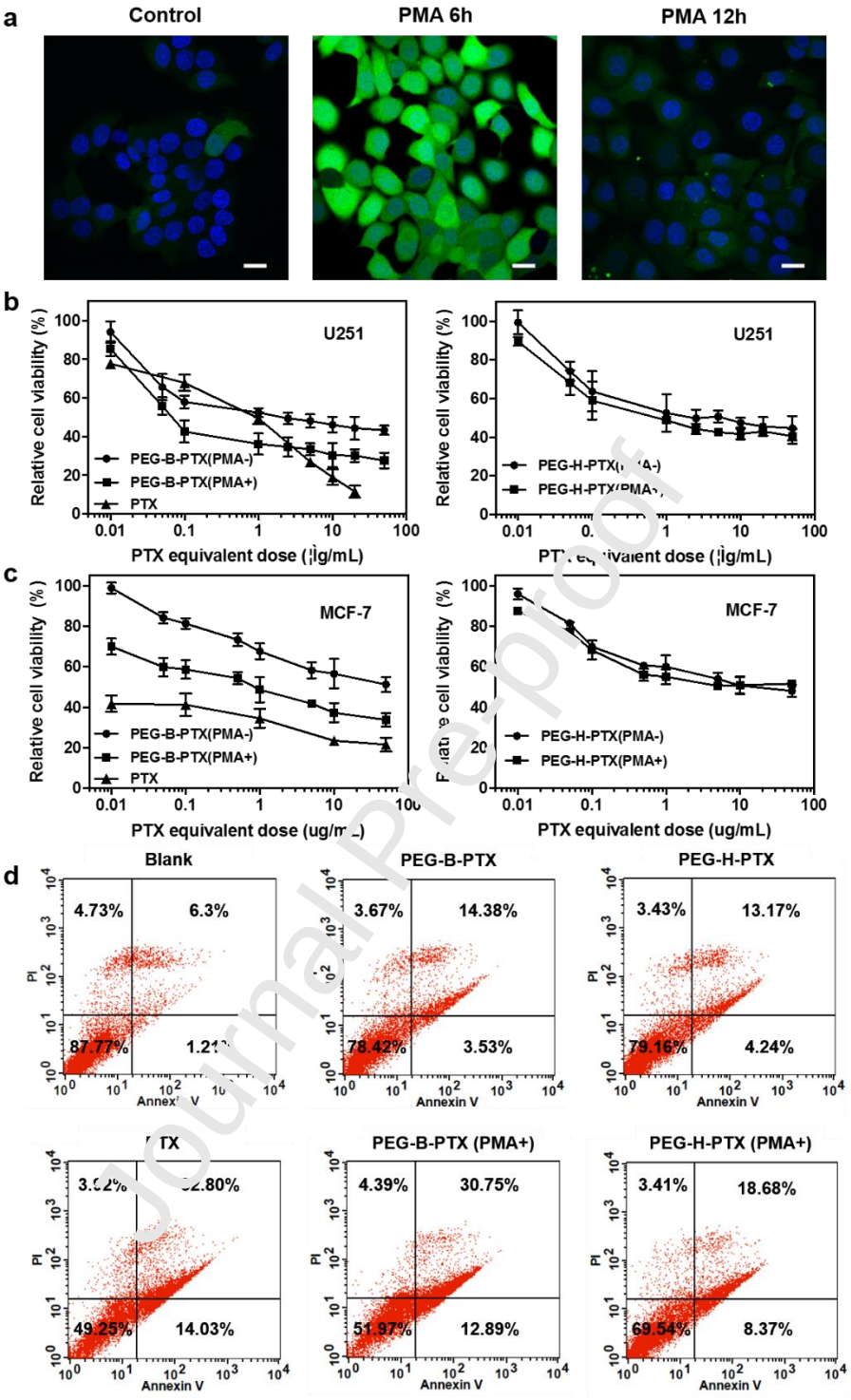

Fig. 3. ROS-dependent cell cytotoxicity. (a) Confocal microscopy images of intracellular ROS generation in MCF-7 cells with or without 200 nM PMA for 6 or 12 h. All scale bars are 20 μm. Cell nuclei are stained by Hoechst 33342 and expressed as blue. 2′,7′-Dichlorodihydrofluorescein (DCF)-induced by ROS is expressed as green. (b, c) Effect of PMA-pretreatment on the cell cytotoxicity of PEG-B-PTX and PEG-H-PTX to U251 cells (b) and MCF-7 cells (c). The cells were pretreated with

PMA (200 nM) for 6 h before the addition of the prodrug and free PTX. (d) The apoptosis of MCF-7 cells was determined by Annexin V/propidium iodide double staining. Cells were treated with PEG-B-PTX or PEG-H-PTX (PTX equivalent dose 5 μg/mL) for 48 h.

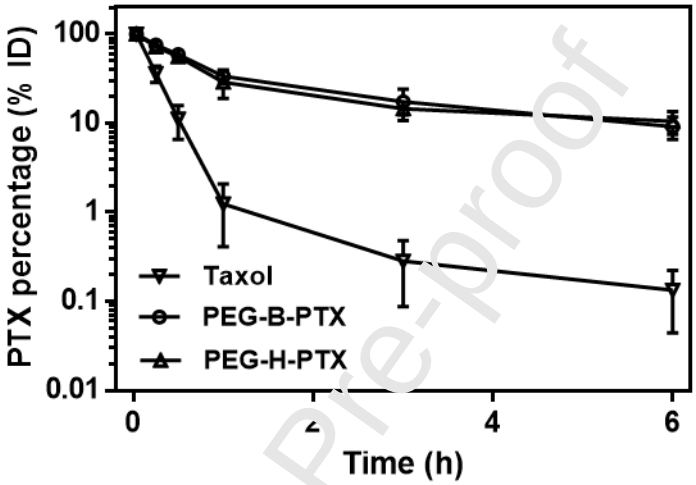

Fig. 4. Blood clearance kinetics of PTX after a single injection of PEG-B-PTX, PEG-H-PTX, and Taxol at a PTX equivalent dose of 10 mg/kg (n = 3).

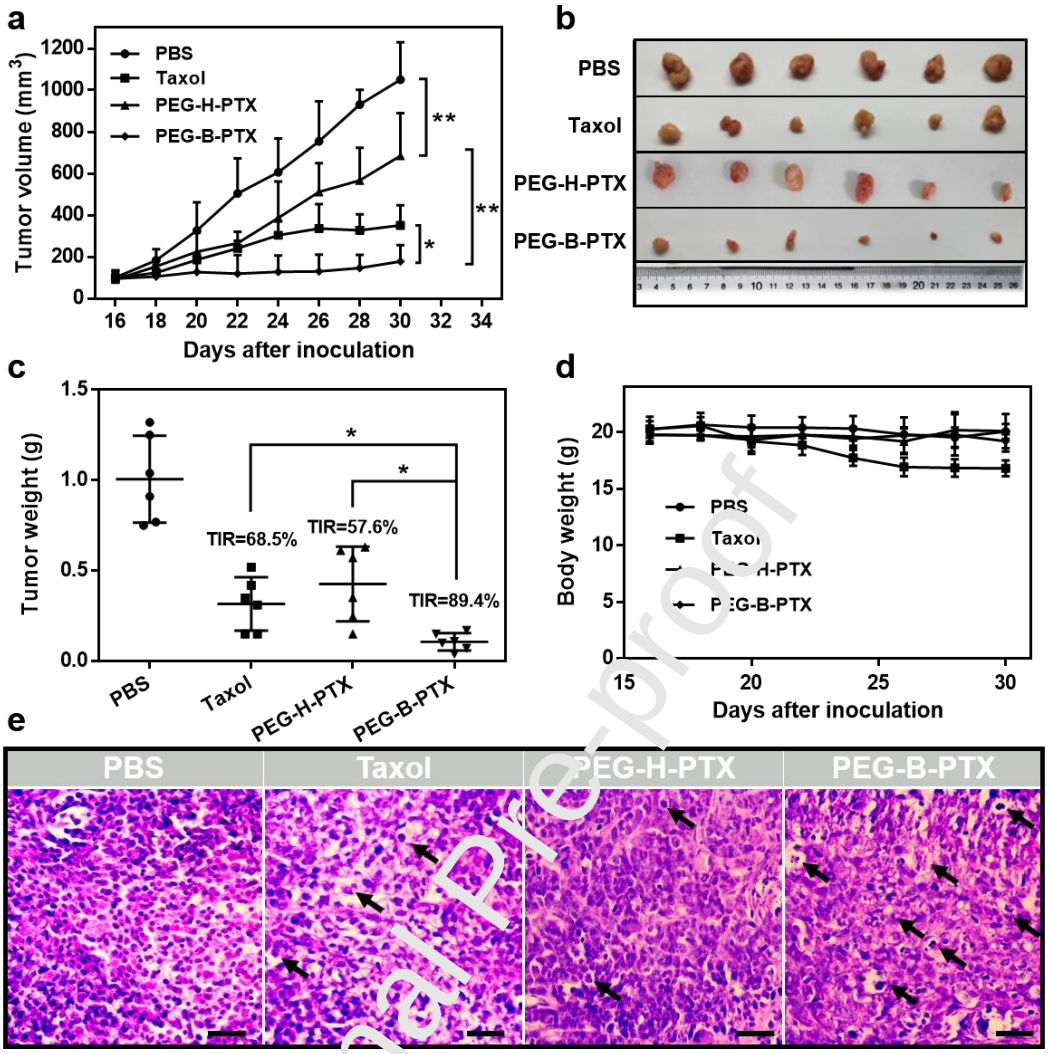

Fig. 5. *In vivo* antitumor activity. (a) The MCF-7 tumor volume changes in mice treated with PBS, PEG-B-PTX, PEG-H-PTX, or Taxol (PTX-equivalent dose 10 mg/kg) with five replicate doses. (b) The average tumor weight of each group at the end of the experiment. (c) The body weight variation of tumor-bearing mice during the treatment (d) Images of the MCF-7 xenograft tumors of the mice at the end of the experiment. (e) Representative histological features of the tumors 7 days after the last treatment. Tissue paraffin sections were 10-μm thick. The tumor sections were stained with hematoxylin–eosin and examined by light microscopy. Scale bars = 50 μm. Error bars indicate s.d. (n = 6). *$P < 0.05$, **$P < 0.01$ (two-tailed Student's *t*-test).

Table 1. Blood half-life and area under the curve for different formulations of ICR mice at a PTX-equivalent dose of 10 mg/kg.

Parameter	Unit	PEG-B-PTX	PEG-H-PTX	Taxol
$T_{1/2}$ alpha	h	0.41 ± 0.03	0.41 ± 0.10	0.10 ± 0.08
$T_{1/2}$ beta	h	4.88 ± 1.61	5.44 ± 2.06	0.18 ± 0.05
$AUC_{0\sim t}$	μg mL^{-1} h^{-1}	153.73 ± 29.20	140.11 ± 16.73	29.63 ± 1.80

$T_{1/2}$ alpha: the half-life of the distribution phase. $T_{1/2}$ beta: the half-life of elimination phases. Data are depicted as mean ± SD. Statistical significance: $^{*}P<0.05$.

Graphical abstract: